Physica A 671 (2025) 130628

Contents lists available at ScienceDirect

Physica A

journal homepage: www.elsevier.com/locate/physa

Cellular automata for the investigation of navigation dynamics and aircraft mix in terminal arrival traffic

Ikeoluwa Ireoluwa Ogedengbe [a,*], Tak Shing Tai [b], K.Y. Michael Wong [c], Rhea P. Liem [d,e,**]

[a] Academy of Interdisciplinary Studies (Intelligent Transportation), The Hong Kong University of Science and Technology, Clear Water Bay, Hong Kong Special Administrative Region
[b] Department of Electronic Engineering and Computer Science, Hong Kong Metropolitan University, Homantin, Hong Kong Special Administrative Region
[c] Department of Physics, The Hong Kong University of Science and Technology, Clear Water Bay, Hong Kong Special Administrative Region
[d] Department of Mechanical and Aerospace Engineering, The Hong Kong University of Science and Technology, Clear Water Bay, Hong Kong Special Administrative Region
[e] Department of Aeronautics, Imperial College London, United Kingdom

ARTICLE INFO

Keywords:
Terminal maneuvering area
Cellular automata
Routing strategy
Arrival traffic mix
Fundamental diagram

ABSTRACT

Investigating the impact of traffic mix and route flexibility on the arrival traffic dynamic within the terminal maneuvering area (TMA) is challenging, mainly due to the spatial constraints and wake turbulent separation requirements. In this study, we capture the dynamism of complex interactions and non-linearity in traffic by using a cellular automaton that is modified to enable more realistic representation of air traffic movements. Our results show that route flexibility makes traffic less sensitive to changes caused by size-based traffic mix and demonstrate the emergence of an organized flow zone in the fundamental diagram of the flexible strategies. When a gentle TMA saturation behavior is preferred, however, less flexible routes are deemed more suitable. As a general principle, we propose to adopt a mixed strategy that uses a fixed routing strategy at low TMA occupancies and a flexible routing strategy at medium to high TMA occupancies.

1. Introduction

Despite the undeniable importance of air transportation, its rapid growth has notably increased traffic congestion that leads to delays, schedule disruptions, environmental hazards (in the form of noise and air pollution), and higher costs associated with increased fuel consumption [1,2]. During arrival, the congestion becomes especially pronounced at the terminal control or terminal maneuvering area (TMA), where traffic begins to converge as aircraft approach the runway. Furthermore, aviation regulations stipulate that there should be a minimum distance (also known as *wake separation minimum*) between adjacent aircraft—where a longer separation is required when the leading aircraft is larger—to prevent disturbances, such as rolling moments, on the follower aircraft behind. Therefore, the aircraft-size distribution (i.e., the *traffic mix*) and the path of aircraft movement within the TMA are critical to the efficient coordination of traffic in a given airspace sector [3]. These operational constraints render modeling and analysis of TMA challenging, which we aim to tackle in this work.

* Corresponding author.
** Corresponding author at: Department of Aeronautics, Imperial College London, United Kingdom.
E-mail addresses: iiogedengbe@connect.ust.hk (I.I. Ogedengbe), stai@hkmu.edu.hk (T.S. Tai), phkywong@ust.hk (K.Y.M. Wong), r.liem@imperial.ac.uk (R.P. Liem).

https://doi.org/10.1016/j.physa.2025.130628
Received 4 November 2024; Received in revised form 28 March 2025
Available online 6 May 2025

Within TMA, an aircraft typically follows a certain arrival route, which is an *airway* defined by a series of waypoints. A *waypoint* is an abstraction of spatial references that can either be named fixes (position markers) or conspicuous physical infrastructure; in some cases, it could also be the destination [4]. Current TMA operations require the explicit coordination of the arrival process—by strictly following waypoints—by air traffic controllers [5]. However, depending on the aircraft's capability (such as the inertial navigation and Global Navigation Satellite System [GNSS]) and air traffic control's guidelines, there could be some *route flexibility* in terms of how much the aircraft is mandated to follow the standard arrival route [6]. A past study has shown that this flexible point-to-point approach can facilitate smoother trajectories [7]. In this work, we want to further investigate how this route flexibility affects congestion evolution inside TMA.

In modeling aircraft arrival traffic performance, considering aircraft size distribution and the flexibility of route selection under different traffic condition is imperative. However, capturing the dynamism of these factors is challenging due to the fairly high number of entities (aircraft) continuously interacting in a dynamic environment and the need to properly model some realistic constraints, such as wake turbulence separation and collision avoidance. Such a modeling challenge requires an equally dynamic abstracting framework for capturing the key aspects of the system.

Modeling the inherent complexity of interactions between aircraft within the TMA under relevant constraints is not new. Early work in TMA modeling focused on understanding the spatial interaction between converging trajectories with multiple aircraft approaching the runway [8]. The next development included the temporal dimension, which made it possible to perform more advanced analyses such as conflict prediction [6], the estimation of the degree of path variability [9], and the detection of trajectory degradation [10]. Effects of ground operations have also been accounted for in some studies [11,12], whilst some others investigated the impact of weather [13,14]. In general, there are three commonly used methods to model arrival traffic within the TMA, namely data-driven modeling (primarily machine learning), network modeling, and arrival sequence modeling. Each of these methods is described briefly below, along with discussion on its limitations.

Machine learning has been widely adopted for trajectory prediction purposes [15], mainly to identify flight trajectory clusters geographically based on directions of arrival [16,17] and derive performance metrics to describe the flow efficiency, airspace capacity utilization, and traffic variability of various TMA configuration [18,19]. Despite these demonstrated successes, the relevance of their results are confined within the design space from which data are obtained, which limits the applicability of these data-driven models to other airports or regions. Furthermore, the large amount of data and a considerable amount of time required to tune, train, and optimize the models might limit its usage in real-time application [20,21].

Alternatively, researchers adopt methods that facilitate the abstraction of trajectories, such as graph networks—which conceptualize point-to-point relationships as vertices and edges [22]—or space–time [23] networks. These models can be used to evaluate traffic mobility by observing the diffusivity of the network. In these methods, the network topology is designed to imitate aircraft flow across the airspace, from point to point, where the edges connecting any two points are weighted according to the volume of the traffic between the nodes [24]. There are three main limitations with these models, namely the limited representation of distance, the lack of visualization capability, and their inability to capture and model sources of uncertainty and non-linearity such as wake turbulence separation. In arrival sequence modeling, this separation is often modeled by adopting the classical queuing model [25,26] or discrete event simulations [27]. However, these sequential models are not suitable to effectively represent the non-linear interactions between multiple aircraft in evaluating different arrival strategies.

From the above discussion, we can conclude that existing approaches still fall short in establishing a generalizable model—that is, one that can be easily implemented in different airports and regions—that can capture dynamic traffic patterns across a wide range of TMA configurations. To be effective and practical, the model needs to be computationally efficient and yet able to represent the interaction between multiple agents—which is typically non-linear—within a constrained environment.

A statistical physics model, particularly the cellular automaton (CA), is deemed suitable to address this need. Such a model mimics the interaction of molecular agents in chemical/atomic species that are driven by subatomic forces generated by neighboring atoms. CA can model the system using the explicit simulation of the dynamics of its components. This 'data-free' approach allows for some flexibility in the boundary conditions that can be explored and excludes some drawbacks associated with poor-quality data. Furthermore, CA facilitates the construction of non-linear, complex interactions between multiple entities from the fundamental principles of system operation. CA has a long history of diverse applications, most prominently in areas such as ground traffic modeling [28], population dynamics [29], crowd evacuation [30], and epidemic spread [29]. This lends credence to its appeal in modeling the dynamics of non-linear physical systems. In our study, each element (waypoint coordinates, different sizes of aircraft) is treated as a distinct entity, with self-contained properties and local dynamics that affect traffic in its neighborhood. Using CA to model arrival dynamics can provide some insight into the interaction between the degree of route flexibility and traffic mix in the onset of congestion during the aircraft arrival process. These effects will be evaluated by observing the variation in flow and speed of arrival traffic over a range of TMA occupancies. Our study reveals the *organized flow phase* that emerges under the flexible route selection strategies, as observed from the fundamental diagram. This is notable for showing the dynamic interaction between the route flexibility along finite paths with the converging flow of aircraft arrival traffic. The results also demonstrate the benefits of a mixed strategy, which comprises adopting a fixed route selection at low TMA occupancies and a flexible one at high TMA occupancies, in improving traffic performance.

The remaining parts of this paper are arranged as follows. Section 2 describes the modification of CA model to be suitable for TMA arrival traffic modeling. Simulation results will be discussed in Section 3; the conclusion alongside possible directions for future work will be presented in Section 4.

2. Methodology

Statistical physics techniques (including CA) primarily focus on systems with many interacting components or agents, providing an essential theoretical bedrock for understanding the emergence of macroscopic properties from microscopic interactions—which is also a central idea in complex systems [31]. The field's aim to explain bulk phenomena (e.g., temperature, congestion) in physical systems as emergent behaviors of many microscopic constituents makes it a natural analogue for understanding complex behavior in traffic systems. Indeed, statistical physics offers the conceptual and mathematical tools, such as statistical ensembles and averages, to analyze the many degrees of freedom inherent in complex systems [32]. By focusing on ensemble averages, statistical physics captures typical and probable behaviors at scale, a crucial approach when dealing with the inherent stochasticity and variability common in complex systems [33].

Key to applying statistical physics is a model that can represent the microscopic interactions between entities, following rules that reflect their behavior in real situations, to a reasonable extent. It is worth noting that to fit into the statistical physics paradigm, the interaction modeling might not follow certain physical rules or governing equations exactly—however, they should be sufficient to provide a faithful abstraction of the underlying system properties/behavior, as will be further elaborated below. Taking an example from road traffic, simple rules governing microscopic interaction at the level of each vehicle (i.e., cell in CA) and its immediate neighbors in a CA framework are known to produce realistic insight into traffic complexity. These rules, obtained from the abstraction of actual road traffic dynamics, typically include acceleration, collision avoidance, random deceleration, and discrete movement. Similarly, in the statistical physics modeling of aircraft arrival traffic, the concepts of aircraft identity, spatial interaction, and wake turbulence separation are conceptualized as abstractions in a CA framework that focus on capturing their essence, rather than their explicit representation. Thus, as we will further highlight in the model scope and assumptions (Section 2.2), TMA configuration and traffic movements in the CA framework are only representative of actual aircraft arrival traffic.

CA is a discrete computation method that is commonly used to model non-linear multi-agent systems [34] by framing the physics of interactions with well-posed dynamics and boundary conditions [35]. In CA, each element can occupy a cell in a grid system, where its Boolean state transition to the next step follows a certain *transition rule* that models the interaction between each cell and its neighbors. The system characteristics can be observed by means of some quantities of interests (e.g., flux, the number of movements, etc.) once the simulation reaches an equilibrium. By using a fundamental diagram, we can observe the *phase transition* as the system crosses a dynamical threshold [36] at a certain *critical point*, which is often linked with the density of the system [37]. Phase transition and critical points can help characterize complex systems [38], specifically by distinguishing different operational modes within a system, such as free flow and congested flow states in ground traffic [39]. CA's appeal is further enhanced by its overall simplicity (albeit non-trivial) and relatively inexpensive computational cost.

Even though CA has been commonly used in ground transportation modeling [28], its implementation in air traffic modeling is not as extensive, due to the higher complexity and more stringent regulations of air traffic movement. In the context of TMA modeling, Wang et al. employed CA to model aircraft navigation within the TMA [40,41]. However, instead of using waypoints as the primary means of navigation, their aircraft movement was driven by obstacle avoidance, without factoring the impact of designated arrival routes. Another example was demonstrated by Yu et al. [42] on aircraft landing scheduling. In particular, they used a fast, one-dimensional representation of the landing queue, without really considering the lateral interaction between trajectories from different TMA entry points. With our current work, we wish to further extend CA's applicability in air traffic modeling by focusing on realistic arrival navigation via waypoints.

To derive a suitable CA model, the traffic movements are represented as a system of interacting particles or entities, where the interaction of these entities in their respective neighborhoods leads to certain route choices and movement dynamics as they move in time and space. By evaluating the neighborhood-based interaction, the system complexity is somewhat reduced to a set of simple rules/decisions at the microscopic level, which are then aggregated to obtain the corresponding system-level dynamics. Furthermore, modeling the fundamental principles of aircraft arrival movements can be applicable in different configurations, as opposed to domain- and data-specific models that have more limited applicability. Hence, the model can be used to enhance our understanding of universal traffic behavior, regardless of the airspace layout.

2.1. CA model formulation for arrival traffic within TMA

The basic elements of our CA TMA model are shown in Fig. 1, including the TMA entry, which always serves as the origin cell; TMA exit, which always constitutes the destination cell; boundary cells, which are always "occupied" to provide a fixed barrier for aircraft movement; and waypoints, which refer to fixed, intermediate destinations within the grid system. To represent the traffic movements within TMA more faithfully, this TMA model has fixed locations for TMA entry and TMA exit (defined as the point where the aircraft is finally cleared for uninterrupted landing), which is different from typical 2D CA simulations where the origin and destination can be set as random [43]. A periodic boundary condition—which is common in CA models [44,45]—is applied between the TMA entry and the TMA exit in order to have a sustained traffic flow for a sufficiently long duration until variables of interest become stable (which is needed to obtain the ensemble averages). It is worth noting that the re-entering entity does not retain its previous identity; instead, it simply represents a new incoming flight to the TMA. By connecting opposite edges of the simulation space, periodic boundaries create a seamless environment, ensuring consistent neighborhoods for all cells and preventing artificial boundary-induced behaviors. This approach is particularly valuable for approximating real-world traffic flows, which occur in large, continuous systems, and for studying intrinsic dynamics like traffic jam formation without boundary interference [39,46]. Moreover, periodic boundaries facilitate the conservation of aircraft within the simulation, thus maintaining constant aircraft density. From

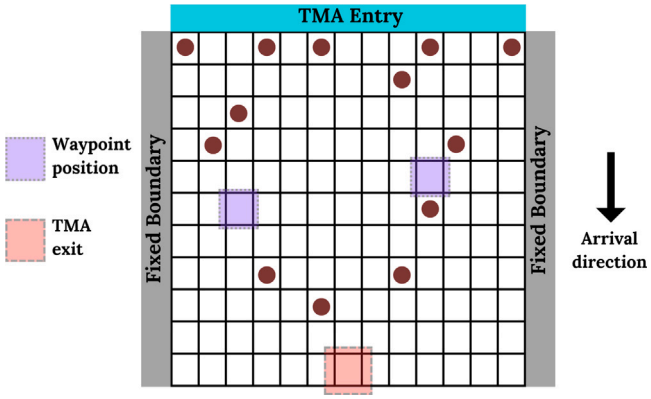

Fig. 1. A conceptual illustration of TMA arrival traffic within the CA framework.

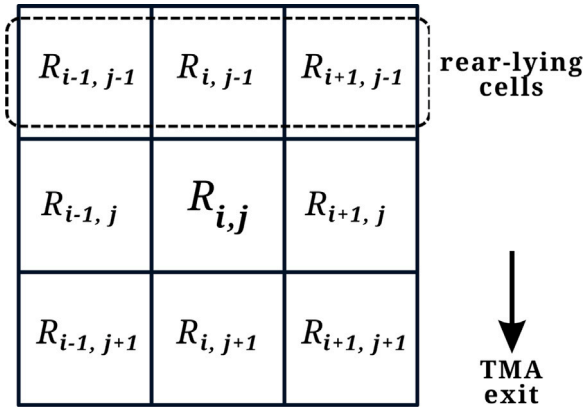

Fig. 2. A conceptual illustration of an aircraft's neighborhood in a 2D CA grid for TMA.

a computational perspective, these conditions streamline the application of CA rules, eliminating the need for special handling of boundary cells.

Key features associated with TMA aircraft arrival include convergence of arrival routes, selection of arrival route (via waypoints), traffic element property specification, and turbulent wake separation. Our model can simulate various traffic states within TMA, upon determining the desired navigation structures and strategies. The simplest case for this setup is that aircraft navigate using the nearest waypoints as they traverse from entry to exit, with limited route flexibility. In other scenarios, we investigate other levels of route flexibility where the aircraft can probabilistically select from several nearest waypoints. Each of these scenarios is simulated for weakly inhibited and strongly inhibited traffic cases with various aircraft size distributions.

To model TMA using CA, the TMA region needs to be represented as a 2D grid (G) with the location and coordinates of a cell denoted as $R_{i,j}$ and $(X_{R_{i,j}}, Y_{R_{i,j}})$, respectively. The state of a cell at time t, $G^t(i,j)$, is defined by its occupancy and is represented as a binary variable:

$$G^t(i,j) = \begin{cases} 1 & \text{if occupied;} \\ 0 & \text{otherwise.} \end{cases} \tag{1}$$

Here, a cell state is one when an aircraft occupies it. For each aircraft g, we associate a weight w_g to differentiate the sizes of aircraft. In this study, we consider four size classes, namely super heavy (SH), heavy (H), medium (M) and small (S). Hence, the weights associated with the size classes are $w_g(SH)$, $w_g(H)$, $w_g(M)$, and $w_g(S)$; where $w_g(SH) > w_g(H) > w_g(M) > w_g(S)$. The neighborhood of cell $R_{i,j}$—which is important in CA transition rule—is shown in Fig. 2, which also shows the rear-lying cells and the direction for the destination, i.e., TMA exit or the final approach fix (FAF). Here, rear-lying cells are defined as cells that lie between the current location and the entry point. As shown in Fig. 2, $R_{i,j}$ has a Moore neighborhood, which consists of the cells that are adjacent to it in all directions.

2.2. Model scope and assumptions

To better represent TMA traffic movements, our CA model explicitly considers diverse arrival population (traffic mix), waypoint-dependent route selection capabilities, and arrival condition variation, which distinguishes it from the conventional, homogeneous

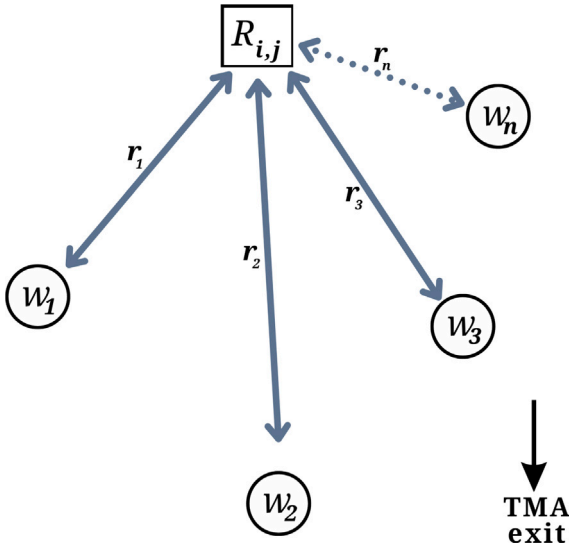

Fig. 3. A depiction of the flexibility based on the proximity of waypoints in the neighborhood of an aircraft.

CA model. In addition, we also introduce some assumptions that are relevant to air traffic modeling, namely (1) there is no back-flow, that is, rear-lying cells are not considered as an aircraft selects the path at each time step; and (2) there are no missed approaches, in that all aircraft entering the TMA get through to the TMA exit in their first attempt. In our model setup, aircraft are uniformly spread out as they come into the TMA such that the arrival traffic is not concentrated in any one side or group of cells at the TMA entry. The path selection is determined solely based on local interactions. Lastly, we limit our modeling scope by conceiving TMA as a single homogeneous entity without any sectorial divisions within the domain. In such a case, we do not model the "transfer of control" between one airspace sector to another, which commonly happens in actual operations.

Recall that the main goal of using statistical physics modeling such as CA is to capture the macroscopic behavior of a complex system based on its inherent microscopic interactions. Hence, instead of aiming for realistic physical representation of TMA configuration and traffic movements, we generate an abstraction of the microscopic interaction between entities (i.e., aircraft) within TMA, from which the macroscopic characteristics are deduced. In this regard, some assumptions and physical limitations implemented in our CA model derivation are briefly described below.

First, the three-dimensional aircraft movements are represented in a two-dimensional space in our TMA formulation. This simplification is commonly performed in other TMA studies [40,47], as it is deemed sufficient to represent critical aircraft operations in many TMA scenarios, including the horizontal separation of aircraft. Second, the simulated movements of aircraft in CA might not faithfully represent the intricacies of realistic flight routes, where aircraft are often directed to perform vectoring or wait in holding patterns to manage aircraft separation and sequencing [48,49]. However, the transition rules implemented in our model—which depend on neighboring cells' occupancy—can represent these maneuvering strategies by design, to a certain extent. There could be instances where the aircraft trajectory must be deflected when some of the neighboring cells are occupied and thus block a straight trajectory towards the next waypoint. This imitates radar vectoring in actual aircraft movement where a path different from the shortest path or standard route may be specified in order to prevent separation violation [50]. When all neighboring cells are occupied, aircraft movement is rendered impossible; this is analogous to the aircraft being put in a holding pattern. A detailed explanation of this mechanism is provided in Section 2.3. Third, the actual waypoint locations within TMA might not be accurately represented in our CA model. However, we position the waypoints in a way that adheres to the characteristics of arrival traffic in the TMA, characterized by their convergence as they get closer to the TMA exit (as reflected in Fig. 1). This will be further described in Section 2.5. Lastly, the number of aircraft included in the simulation might seem to be much higher than the realistic capacity of actual TMA (which typically varies between 20 and 40 per hour for arrival at most airports [51]). The high number of aircraft agents is necessary to model microscopic interactions within TMA, in order to obtain the ensemble averages. In this case, the maximum occupancy modeled in CA does not correspond to the situation where aircraft fully occupy the airspace; instead, it represents the maximum capacity of TMA, while satisfying the minimum distance between aircraft and other regulatory requirements.

2.3. Model features

Our model features are designed to emulate the essential aspects of aircraft arrival traffic. The interpretation of each feature is presented as follows:

Path Convergence and Route Selection: An arrival route is modeled by directing aircraft to follow a sequence of waypoints, based on the specified level of route flexibility. This is captured by the *flexibility index*, which will be described below using the

illustration shown in Fig. 3. In the figure, we have an aircraft at a position $R_{i,j}$ at time t, and the distances of this aircraft from waypoints w_1, w_2, …, w_n are r_1, r_2, …, r_n respectively. In the illustration shown in Fig. 3, we have $r_1 < r_3 < r_2$. The flexibility index is defined as the maximum number of closest waypoints the aircraft may head towards in the next time step from its current position in the TMA. Thus, if the aircraft considers only the closest waypoint, the flexibility index is 1 (first order, F1), in which case the route selection is fixed. Under this scenario, the aircraft shown in Fig. 3 will go to w_1 at the next time step. Under the more flexible F2 condition (second order), it can consider going to w_1 or w_3 at the next time step, according to some predetermined probability distribution. Following the same rationale, all three waypoints are considered under the F3 case. Note that the route flexibility index can be a higher number; three is used here only for illustration purposes.

At each time step, the origin–destination (OD) pair is defined by the current position of the aircraft and the selected waypoint as the origin and destination, respectively. For any aircraft g at any time t, r_g^t is a distance-based property used to determine the nearest waypoint,

$$r_g^t = \arg\min_{n\in\{W_G\}} \sqrt{(x_g^t - x_n^t)^2 + (y_g^t - y_n^t)^2}, \tag{2}$$

where x_g^t and y_g^t are the aircraft's origin-referenced coordinates, respectively; x_n^t and y_n^t are the coordinates of waypoint n (where n belongs to the set W_G of all waypoints in grid G).

Aircraft Movement: Once the flow direction is established, we define the transition rules of cell $R_{i,j}$ (to time $t+1$) with two phases. First, the aircraft has to identify the potential cell m in its neighborhood. As a way to ensure the *no back-flow* condition is met, we assume that its rear-lying cells are occupied with virtual aircraft, i.e., $G^t(i-1,j-1) = G^t(i,j-1) = G^t(i+1,j-1) = 1$. Given this condition, we may rewrite the *effective neighborhood* $M_{i,j}$ of $R_{i,j}$ as:

$$M_{i,j} = \{R_{i+k_1,j+k_2} | k_1 \in \{-1,0,1\}, k_2 \in \{0,1\}, |k_1| + |k_2| \neq 0\}. \tag{3}$$

Among the cells in $M_{i,j}$, only the unoccupied ones are considered for the next movement, since one cell cannot be occupied by multiple aircraft. We denote the unoccupied cells in $M_{i,j}$ as $M_{i,j}^{\mathrm{u}}$ (correspondingly, the occupied ones are denoted as $M_{i,j}^{\mathrm{o}}$). We then determine the closest cell relative to the selected waypoint, denoted by q_m^t, as

$$q_m^t = \arg\min_{m\in\{M_{i,j}^u\}} \sqrt{(x_m^t - X_{r_m^t})^2 + (y_m^t - Y_{r_m^t})^2}, \tag{4}$$

where x_m^t and y_m^t are the origin-referenced coordinates of m at time t, whereas $X_{r_m^t}$ and $Y_{r_m^t}$ are for the selected waypoint r_m^t in Eq. (2). In a case where there are multiple cells that fit the minimum distance criterion, one of them is chosen at random.

The second phase handles the wake turbulence separation requirement, which is modeled heuristically to align with the statistical physics paradigm. In particular, this requirement is manifested by defining a transition probability as a function of aircraft size distribution among the occupied cells in $M_{i,j}^{\mathrm{o}}$. This transient probability would deter aircraft from moving when there are larger aircraft around, akin to keeping a longer distance behind a larger aircraft. To gauge the aircraft size distribution, we first evaluate the weighted sum S_w of occupied cells in $M_{i,j}^{\mathrm{o}}$, which is a function of the aircraft size indicator w_g. Considering all occupied cells g in $M_{i,j}^{\mathrm{o}}$, the weighted sum is defined as

$$S_w = \sum_{g\in\left\{M_{i,j}^{\mathrm{o}}\right\}} w_g \cdot G_g^t. \tag{5}$$

It is worth noting that S_w implicitly contains information about local density, since it considers all occupied cells in the vicinity. We set thresholds a_1 and a_2 for the value of S_w to simulate wake turbulence separation. For the specified thresholds, we assign a corresponding transition probability, π_T. This transition probability determines whether aircraft movement actually occurs or the aircraft maintains its position. The relationships between π_T and S_w as functions of a_1 and a_2 are shown below,

$$\pi_T = \begin{cases} \pi_1 : & S_w \le a_1; \\ \pi_2 : & a_1 < S_w < a_2; \\ \pi_3 : & S_w \ge a_2, \end{cases} \tag{6}$$

where $a_1 < a_2$ and $\pi_1 > \pi_2 > \pi_3$. The values of π_T, S_w, a_1, and a_2 are calibrated such that for lower thresholds (when S_w is low), the probability of movement π_T is high. This corresponds to a situation where the neighborhood of $R_{i,j}$ is dominated by small aircraft and/or the aircraft are sparsely distributed locally. On the other hand, when S_w is high, the probability of movement π_T is low—this occurs when the neighborhood of $R_{i,j}$ is dominated by large aircraft, especially when the local density is higher. Whilst this approach might not explicitly model the interaction between leading and following aircraft when considering wake turbulence separation, its heuristic nature would yield the ensemble averages that capture the impact of aircraft size on separation distance between aircraft—which serves to achieve the objective of statistical physics modeling.

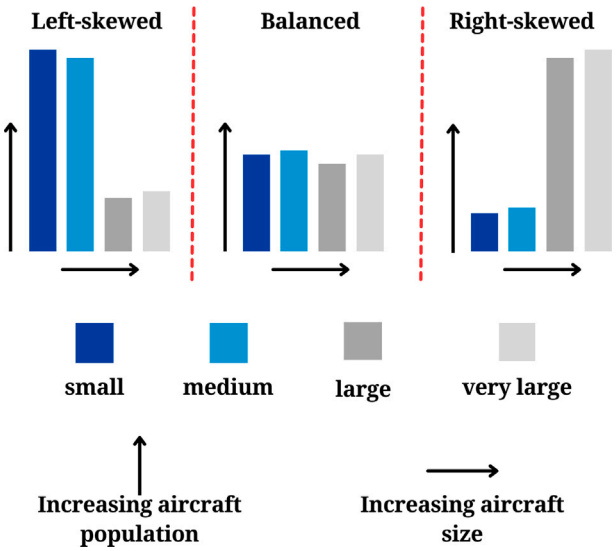

Fig. 4. A depiction of the skewness in arrival traffic based on aircraft size.

2.4. Model parameters

The model parameters enable us to vary simulation conditions in order to capture different operation scenarios. These parameters are associated with the traffic features of interest, namely size distribution (using the skewness in aircraft size distribution) and route flexibility (using the flexibility index described in Section 2.3). The traffic skewness refers to the dominant aircraft size in a given traffic. Fig. 4 shows scenarios when the traffic is dominated by small and medium aircraft (leftmost), distributed quite evenly among sizes (middle), and dominated by large and very large aircraft (rightmost).

In this study, the arrival dynamics will be evaluated under weakly and strongly inhibited traffic conditions. In the weakly inhibited traffic condition, aircraft arrival occurs under nominal conditions, and aircraft follow the baseline wake turbulence separation closely. On the other hand, in the strongly inhibited condition, events such as poor visibility under visual flight rules or bad weather precipitate caution in aircraft agents. As a result, they are mandated to maintain a conservative distance between each other, with air traffic controllers usually increasing the threshold for wake turbulence separation [52].

2.5. Throughput evaluation

We use two metrics to evaluate the throughput of the model under different arrival conditions, namely traffic flow—which relates to the mobility of vehicles—and TMA occupancy—which reflects the space utilization relative to the number of vehicles diffusing through the system. We also examine the average traffic speed to gauge transient traffic behavior. All these are described as follows.

Traffic flow We define the *traffic flow* (q) as the average volume of aircraft going through the TMA space over simulation time. It is a measure of aircraft mobility vis-á-vis the spatial distribution of aircraft traffic under a given arrival condition. This is captured by the average number of movements per aircraft (m_n^t) that take place within a simulation case,

$$q = \frac{1}{T}\sum_{t=1}^{T}\sum_{n=1}^{N} m_n^t, \tag{7}$$

where T is the total number of time steps for a simulation and N is the total number of aircraft in the simulation. The count of m_n^t depends on the change in the cell occupancy, denoted by $\Delta G^t(i,j) = |G^t(i,j) - G^{t-1}(i,j)|$, such that:

$$m_n^t = \begin{cases} 1 & \text{if } \Delta G^t(i,j) = 1; \\ 0 & \text{otherwise.} \end{cases} \tag{8}$$

TMA occupancy We define the *TMA occupancy* (μ) as the ratio of the number of aircraft traversing the TMA to the number of aircraft that saturates the *effective TMA*, to reflect the aircraft density for a given TMA configuration. Given the convergent nature of arrival traffic, the polygon shape of TMA, and a single exit point (see Fig. 5), there are portions of the TMA that are hardly traversed by traffic; these parts are regarded as *dead zones*, which are excluded from the effective TMA. It should be noted that even after the traffic is saturated, limited aircraft movement along the border of the effective TMA and dead zones may constitute extra traffic, resulting in a non-zero flow saturation. One might also argue that this makes practical sense for aircraft traffic, where there is never a complete stoppage of traffic in the air. We will plot the traffic flow against

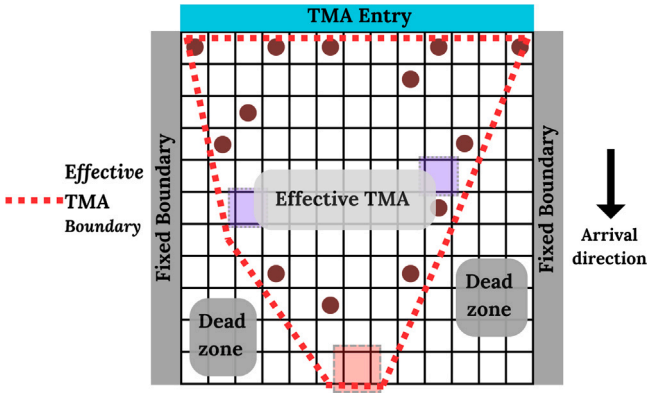

Fig. 5. A depiction of the *effective TMA* and *dead zones*.

TMA occupancy under different conditions in a manner similar to the fundamental diagram used in ground traffic [53], which will be presented in Section 3.

Average traffic speed We define the *average traffic speed* ($\bar{s}$) as the ratio of traffic flow to the number of aircraft that are currently inside the TMA, to indicate how fast the overall traffic is transiting. We follow the same formulation as that for ground traffic [43],

$$\bar{s} = \frac{q}{n}. \tag{9}$$

We will plot the average traffic speed against the TMA occupancy across different cases to describe the traffic behavior.

Evaluating these metrics will help us understand the effect of the parameters being investigated under different arrival conditions. In Section 3, we will present the simulation outcomes, along with relevant discussions.

3. Results and discussion

In this section, we present the results of our simulations across the two features examined, namely size distribution and route flexibility, as discussed in Section 2.4. Three flexibility indices, namely first, second, and third order flexibility (F1, F2, and F3, respectively), are considered in the main simulation cases. The grid size for the simulation is 40 cells by 25 cells. All cases are simulated with 11 waypoints, which are placed such that they facilitate the convergence of traffic on the TMA exit as described in Section 2.2. The locations of these waypoints are fixed for each simulation. The number of time steps per simulation is 10^4 steps, and each data point is obtained by averaging 20 repetitions of each simulation to reduce the effect of randomness. To distinguish different size classes, we assign the following weight values: $w_g(SH) = 4$, $w_g(H) = 3$, $w_g(M) = 2$, $w_g(S) = 1$, and the thresholds a_1 and a_2 are set to be four and eight, respectively. For each feature set, two traffic scenarios are examined, namely weakly inhibited and strongly inhibited traffic. For the weakly inhibited scenario, the transition probabilities are higher, and their values are $\pi_1 = 0.9$, $\pi_2 = 0.7$, and $\pi_3 = 0.5$. For the strongly inhibited scenario, the transition probabilities are set to $\pi_1 = 0.7$, $\pi_2 = 0.5$, and $\pi_3 = 0.3$.

The flow (q) and TMA occupancy (μ) for the model features under different conditions are plotted and subsequently discussed in Sections 3.1 and 3.2. Typical q-μ plots (also known as fundamental diagrams) obtained in this study are shown in Fig. 6 for illustration purposes, which exhibit several distinct zones, including (1) free flow zone, where traffic flow rises steeply with TMA occupancy; (2) congested flow zone, where traffic flow drops rapidly as the TMA occupancy further increases; (3) organized flow zone, where traffic flow rises momentarily as aircraft organize/cluster around waypoints, making some room for mobility; and (4) saturated flow zone, where traffic flow decreases steadily as the effective TMA becomes saturated. As discussed in Section 2.2, the high occupancy shown in the fundamental diagrams presented in this paper is analogous to a situation where the TMA has reached its maximum capacity. In other words, it is more a microscopic representation of traffic saturation rather than having aircraft fully occupying the airspace.

A notable feature of interest in Fig. 6 is the point of maximum flow, also known as the point of *critical occupancy* (μ_c), beyond which an abrupt flow change is observed. The post-peak trend captures the congestion and saturation behavior of traffic. Our simulations exhibit two kinds of post-peak behavior, namely a monotonously decreasing post-peak trend (Fig. 6(a)) and a non-monotonously varying post-peak trend (Fig. 6(b)). Other notable features are the post-peak flow reversal points, μ_1 and μ_2 (as shown in Fig. 6(b)). Detailed explanations on their cause and implications will be presented in Sections 3.1 and 3.2. Supplementary discussions on the transition flow behavior relative to the arrival conditions considered are subsequently provided in Section 3.3.

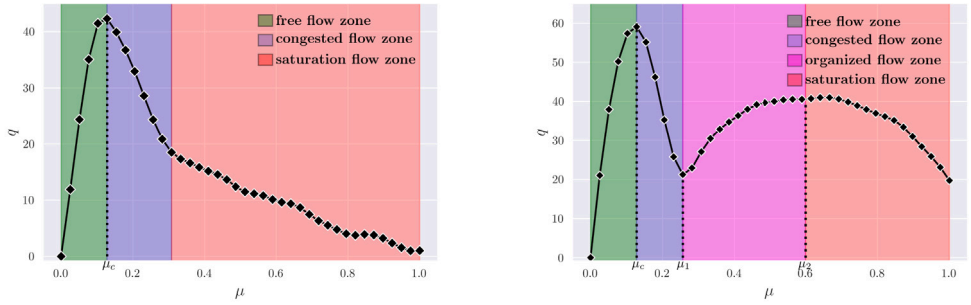

(a) Fundamental diagram with monotonously decreasing post-peak trend

(b) Fundamental diagram with non-monotonous post-peak trend

Fig. 6. Types of fundamental diagrams for different arrival strategies.

3.1. *Effects of size distribution*

Upon observing all cases (as shown in Fig. 7), the left-skewed traffic is shown to have the highest flow, followed by balanced traffic, while right-skewed traffic has the least flow. This is attributed to the spacing dynamics per unit distance associated with each traffic mix. The case with left-skewed traffic has the least cumulative turbulent wake separation between adjacent aircraft because small aircraft require less separation. As a result, it allows for a higher traffic volume in the TMA. On the other hand, the case with the right-skewed traffic has the least throughput due to the higher spacing requirements.

For the F1 case (first order flexibility index, shown in Figs. 7(a) and 7(b)), the pre-peak and post-peak flow characteristic is gentler than in other cases (shown in Figs. 7(c)–7(f)), with a gradual transition from free-flowing to congested traffic. We also observe the smooth curve of the average traffic speed for this configuration in Fig. 9(a). In this state, traffic has a monotonically decreasing post-peak flow behavior, as TMA occupancy is increased beyond μ_c. Under this condition, traffic transits gently from the critical point μ_c to flow congestion and traffic saturation, unlike other cases with F2 and F3 in Figs. 7(c)–7(f). The gentle sloping behavior could be attributed to the orderly nature of the first order flexibility index. Since aircraft explore only one route option via the closest waypoint, the traffic stream settles into and maintains fixed paths. This means aircraft move along relatively fixed trajectories throughout the simulation, depending on their starting positions. This fixity of choice results in slow congestion build up and excludes the dynamic conditions that could lead to an abrupt onset of congestion.

With higher order flexibility indices, F2 and F3 (Figs. 7(c)–7(f)), the pre-peak flow is identical between different traffic mix at low μ. A clear distinction between the flows of different size distributions only begins to appear as we approach μ_c. This behavior may be attributed to the prevalence of a dynamic routing strategy at low μ, i.e., when the TMA is sparsely populated and the effect of the flexible routing strategies of F2 and F3 dominates traffic. Consequently, the impact of inter-aircraft spacing due to size distribution is minimal. This is because the freedom of movement here ($\mu \ll \mu_c$) means aircraft are free to migrate towards adjacent waypoints if there is a space constraint along the route that is associated with the closest waypoint. However, as μ gets closer to the critical flow point ($\mu \approx \mu_c$), the effect of size distribution becomes more prominent, and we see distinct flow curves for each size distribution. Beyond the peak flow point for F2 and F3 cases, the flow drops sharply and then rebounds briefly before flow congestion eventually sets in. The sharp drop after the critical flow point can be attributed to the conflict between aircraft that are actively exploring route options. Within this region ($\mu_c \leq \mu \leq \mu_1$, referring to the illustration in Fig. 6), there is just enough space to explore route options, but very little constraint/incentive to prefer one route over others, depending on the degree of flexibility. This TMA-wide freedom leads to an accumulation of conflicts that reduces flow momentarily. Nevertheless, as μ is increased beyond μ_1, there is less space available for exploration, which forces aircraft to *choose* a preferred route. While this may lead to the clustering of aircraft around waypoints (as illustrated in Fig. 8(b) and will be explained below), it imparts a measure of organization and leaves some space for exit-bound traffic in other parts of the TMA. This dynamic organization of traffic leads to the momentary increase in flow between μ_1 and μ_2. Given the fact that arrival routes are mostly established and the TMA is fairly saturated at this point, the slope between μ_1 and μ_2 is gentler compared to the slope in the free flow zone before μ_c.

Visually observing Fig. 7 suggests a strong similarity exhibited by the trends and behavior of traffic pertaining to F2 and F3 cases. To understand this phenomenon, we will further investigate the effect of flexibility index on TMA traffic dynamics, which will be presented in Section 3.2.

The interesting presence of the organized flow zone (as observed in Figs. 7(c)–7(f)) will be further elaborated below, with illustrations provided in Fig. 8. Note that the aircraft distributions shown in Fig. 8 are exaggerated for clearer illustration purposes—the key aim is to illustrate the presence of the organized flow state prior to saturation. We would like to highlight that they are not our simulation results, and the numbers of aircraft shown in Fig. 8 are arbitrarily chosen to represent different states of CA TMA, which might not correspond to actual TMA situation. The dynamics of transition from free flow (Fig. 8(a)) to saturated flow (Fig. 8(c)) in our simulation of aircraft arrival traffic via the organized flow zone is reminiscent of the three-phase traffic theory

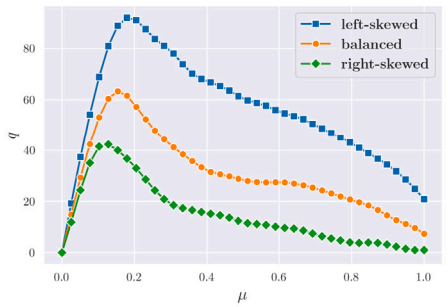

(a) F1, weakly inhibited traffic

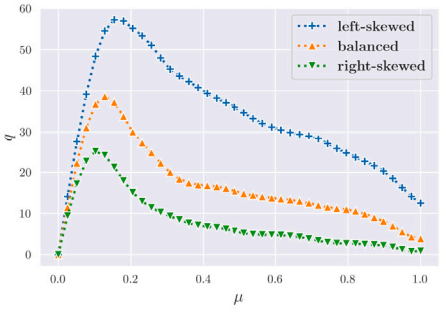

(b) F1, strongly inhibited traffic

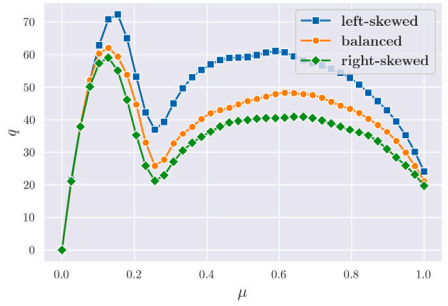

(c) F2, weakly inhibited traffic

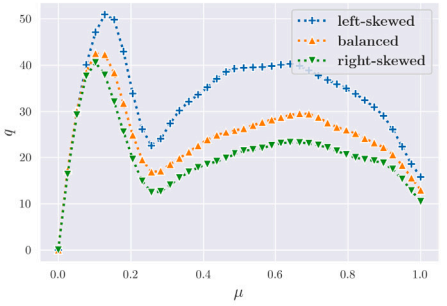

(d) F2, strongly inhibited traffic

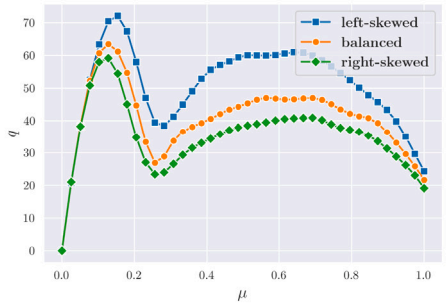

(e) F3, weakly inhibited traffic

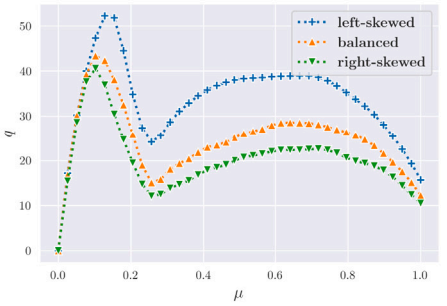

(f) F3, strongly inhibited traffic

Fig. 7. Effect of size distribution on flow behavior for different flexibility indices.

proposed by Kerner in his analyses of road traffic [54,55]. Traditional traffic theory only identifies two phases, namely free flow phase and congested flow phase. However, Kerner observed a third phase, i.e., the *synchronized flow phase*. Kerner opined that the synchronized flow phase in road traffic is the base condition from which traffic jam eventually develops. In other words, traffic does not spontaneously go from free flow phase to congested flow phase. Rather, the synchronization of vehicle speeds downstream of a bottleneck constitutes the *breeding ground* for the development of traffic jam in the congested phase. Similarly, the progression of traffic from free flow state to saturated flow state in our simulation of arrival traffic also goes through an intermediate phase by means of the organized flow state. This phase is characterized by the clustering of aircraft around waypoints and the TMA exit (as shown in Fig. 8(b)), akin to the "bottleneck situation" in the ground traffic case. Furthermore, the synchronization of vehicle speeds during the synchronized flow phase in road traffic is comparable to the synchronization of aircraft headings in the vicinity of waypoints during the organized flow state of TMA arrival traffic. As TMA occupancy is increased beyond μ_2, the spaces between aircraft clusters around waypoints fill up, which leads to TMA saturation. This mechanism of saturation vividly depicts congestion development *precipitated by the nucleation* of aircraft around waypoints.

Another interesting observation is the considerable gap between the flow characteristic of different size distributions for the F1 case (Figs. 7(a)–7(b)). This may be attributed to the absence of lateral route deviation along the arrival routes when this strategy

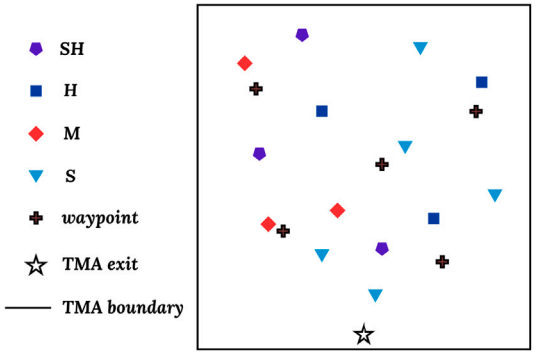

(a) Sparsely distributed traffic in free flow state, $\mu < \mu_c$

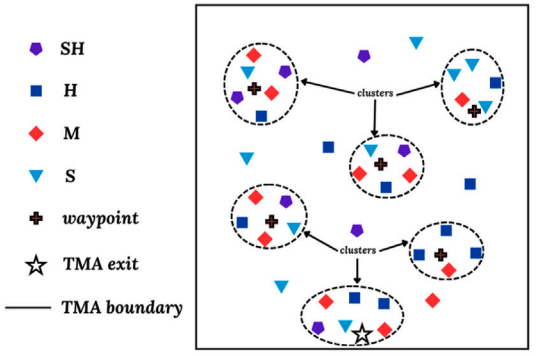

(b) Traffic clustering around waypoints and the TMA exit in organized flow state, $\mu_1 < \mu < \mu_2$

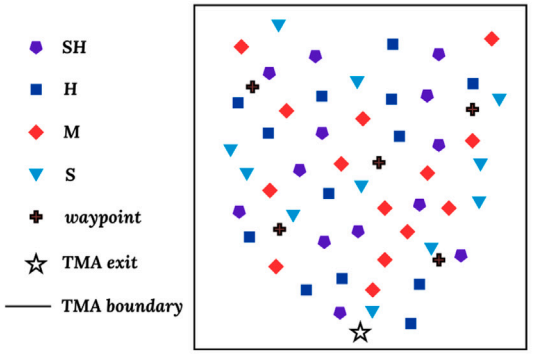

(c) Densely distributed traffic in saturated flow state, $\mu > \mu_2$

Fig. 8. Illustration of the evolution of flow states for F2 and F3 cases (not simulation results). The number of aircraft and their distributions are exaggerated for illustration purpose, with its saturation representing the maximum capacity of TMA (as described in Section 2.2).

is adopted, which amplifies the dynamics of size-based traffic mix. Thus, the effect of size differences is most pronounced in the F1 case. However, the gap between the flow characteristic of higher order flexibility indices (F2 and F3) is less pronounced because the availability of alternative routes dilutes the effect of size distribution. The randomness of route selection that route exploration introduces appears to eliminate the clear impact of size distribution. While still considering the difference in flow behavior across different size distributions, we also observe that the flow curve of left-skewed traffic appears to be further away from balanced traffic than the flow curve of the right-skewed traffic. This asymmetry indicates a possible non-linearity of traffic behavior. A likely cause of this asymmetry is that traffic efficiency scales with less inter-aircraft spacing. Thus, an approximately linear increase in inter-aircraft spacing may lead to a significantly less flow, exceeding the expected proportionality.

Fig. 9 shows the different speed patterns under different traffic conditions, highlighting the size distribution effect on the F1 case (shown in Fig. 9(a)). For the size distributions under the F2 and F3 cases (Figs. 9(b) and 9(c)), a measure of randomness in route selection overshadows size distribution effects (especially at low μ), such that the difference between the average speeds is reduced, compared to the F1 case. It is also observed that the transition from steep to gentle speed reduction differs for the fixed (F1) and

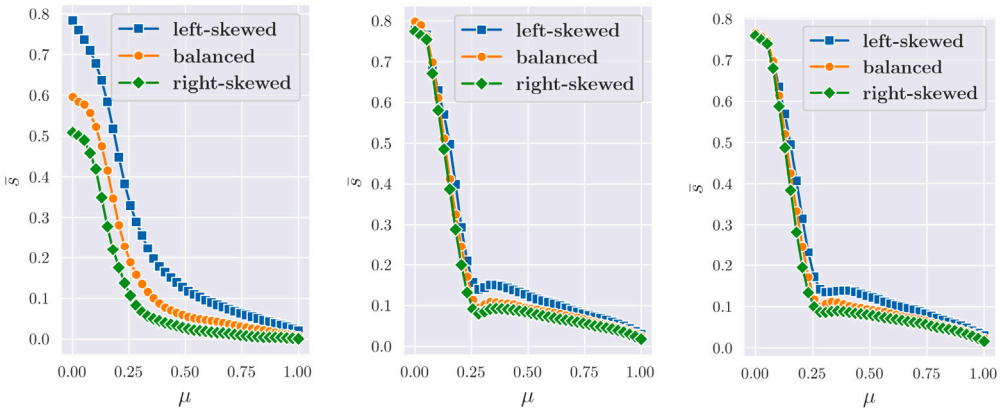

Fig. 9. Average traffic speed for different size distributions at different flexibility indices.

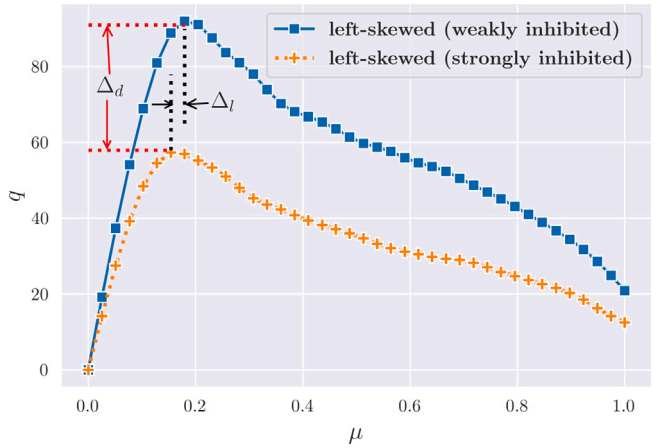

Fig. 10. A depiction of the differences between the weakly inhibited and strongly inhibited cases of the F1 strategy.

flexible (F2 and F3) strategies. The F1 case transitions smoothly because of the *'nearest waypoint'* strategy it adopts. However, the F2 and F3 cases have *kinks* in their *transition elbow*—a feature that may be attributed to the organized flow phase associated with this flow region of the flexible strategies.

Fig. 10 highlights the difference between the fundamental diagrams of the weakly inhibited and strongly inhibited cases, based on the outcomes observed in Fig. 7. It superposes two cases of the fixed strategy, namely a weakly inhibited case (Fig. 7(a)) and a strongly inhibited case (Fig. 7(b)), for easier observation of the flow features affected by traffic inhibition. From Fig. 10, we can observe that increased traffic inhibition results in flow reduction. The cautionary approach required under the strongly inhibited arrival condition leads to mobility restrictions that generate fewer movements throughout the entire simulation. This causes a downward shift of the flow curve, as depicted by Δ_d. Additionally, we observe a leftward shift in the position of μ_c, as depicted by Δ_l. The leftward shift of μ_c implies that traffic congestion appears earlier in the strongly inhibited case and that TMA capacity utilization is less in the strongly inhibited case. This may be attributed to the fact that increased traffic inhibition reduces the tendency of aircraft to explore more parts of the TMA, leading to the occurrence of μ_c at a lower TMA occupancy value.

3.2. Effects of flexibility index

Figs. 11(a)–11(f) compare different route flexibilities, when the traffic is simulated under different size distribution conditions. One key observation here is the notable downward shift in the flow characteristics of F1 across different size distributions. Clearly, fixed arrival strategy exhibits the greatest sensitivity to size distribution under arrival traffic conditions. As inferred in Section 3.1, this may be attributed to the fact that the fixed strategy precipitates limited interaction between aircraft navigating across different waypoints. The minimal route interaction leaves ample space for maximizing the effect of the proportion of different aircraft sizes present in traffic.

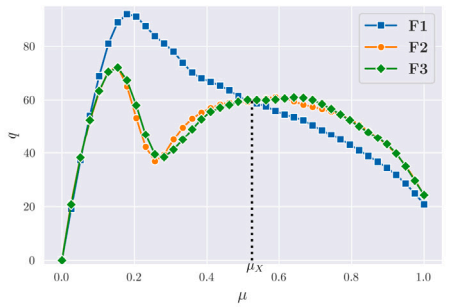

(a) Left-skewed, weakly inhibited traffic

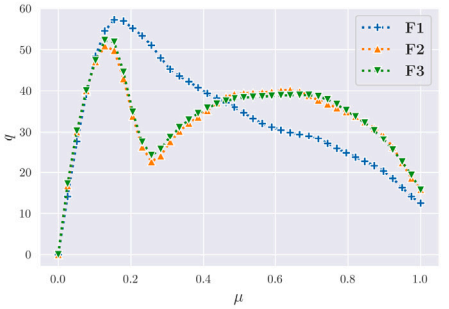

(b) Left-skewed, strongly inhibited traffic

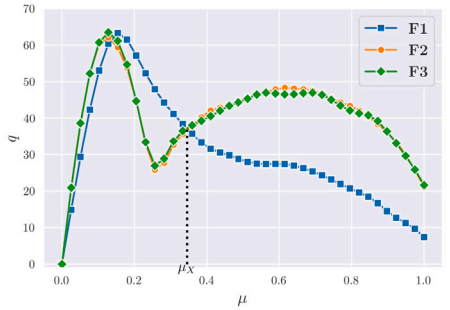

(c) Balanced, weakly inhibited traffic

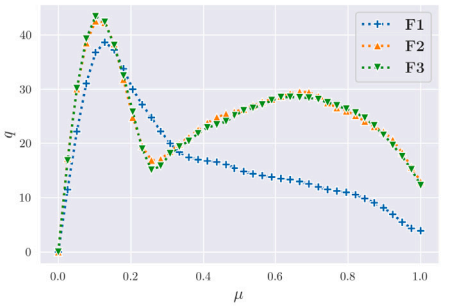

(d) Balanced, strongly inhibited traffic

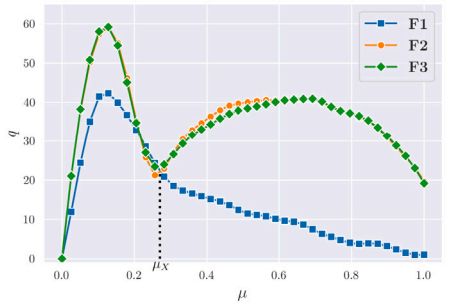

(e) Right-skewed, weakly inhibited traffic

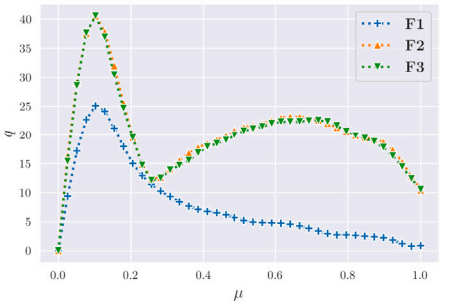

(f) Right-skewed, strongly inhibited traffic

Fig. 11. Effect of flexibility index on flow behavior for different size distributions.

For left-skewed traffic, we observe that all three cases with different flexibility indices appear to have similar flow characteristics at low μ. This implies that route flexibility has little impact on sparse traffic dominated by small aircraft, where every aircraft tends to navigate using the nearest waypoint. Under these conditions, the dynamic influences present within traffic do not trigger route exploration. This is because the ample space available and the lax spacing requirements do not compel aircraft to migrate towards adjacent waypoints. As we approach μ_c, the dynamics of route exploration kicks in, revealing a difference in flow between different flexibility indices. The flow in F1 case continues to increase momentarily, while those of the F2 and F3 cases peak shortly after separation and drop afterward. Also, we see that the F1 case (fixed strategy) has the highest flow, compared to the F2 and F3 cases (more flexible strategies). This may be attributed to the streamlining of arrival routes in the F1 case. In other words, since aircraft only navigate following the closest waypoint, there is no chance of interacting with adjacent waypoints. Given this limited inclination to explore farther waypoints, the aircraft encounter minimal deviation in their heading, as well as a notable reduction in conflicts. As the respective mechanisms of congestion set in, the flows of the fixed and flexible strategies cross each other at μ_X, which approximately coincides with μ_2. Beyond μ_X, the flexible routing strategies exhibit a better flow behavior than the fixed routing strategy. The higher flow of the flexible strategies beyond μ_X may be attributed to the reorganization of traffic around

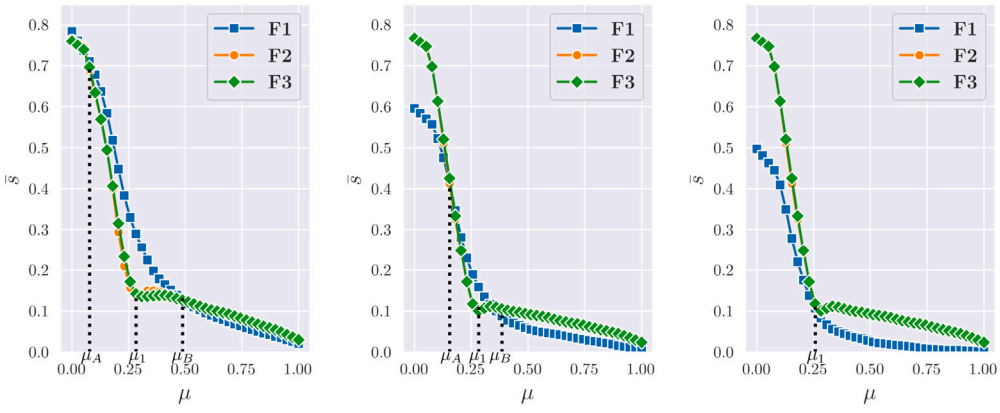

(a) Left-skewed traffic average speed (b) Balanced traffic average speed (c) Right-skewed traffic average speed

Fig. 12. Behavior of average traffic speed for different flexibility indices at different size distributions.

waypoints (which begins at μ_1) that are not necessarily the closest to each aircraft. This leaves some space for areas further away from each waypoint for exploration, leading to an overall gain in traffic throughput.

In the case of balanced traffic, the flow characteristics of the fixed (F1) and flexible (F2 and F3) cases at low μ are not identical. The F1 case has a slightly gentler slope in this free flow phase. However, we observe that the critical flow values of the three cases are similar, compared to the left-skewed traffic where the critical flow for F1 case substantially exceeds those of the F2 and F3 cases. These observations further highlight the greater sensitivity of the fixed arrival strategy to size distribution. The close similarity of the flow characteristics across different flexibility indices up to μ_c indicates that the effect of balanced traffic is mostly uniform across board before flow transition occurs. Beyond the critical point, there seems to be a shift in the traffic dynamics as the flow drops gently and monotonously for the F1 case, whereas the drops are more rapid and dynamic in the F2 and F3 cases. This change in flow dynamics, as well as the radical downward shift in the peak of F1 leads to a shift in the crossover point μ_X away from μ_2 but closer to μ_1. Within the region where $\mu > \mu_X$, we also observe that the flexible strategies exhibit a much better flow behavior than the fixed strategy. This naturally follows from the reduced peak flow of the fixed strategy (the F1 case).

Examining right-skewed traffic, we observe that there is considerably more deviation between the flow characteristics of the fixed and flexible strategies at low μ. This is followed by a rapid peaking of F1 case, while F2 and F3 cases go on to attain a much higher maximum flow at a much steeper rate. The rapid down-shifting and the changing post-peak dynamics of F1 case make μ_X coincide with μ_1, such that most TMA occupancies beyond the critical point yield better flow performance with F2 and F3.

Comparing the strongly inhibited and weakly inhibited traffic cases, the overall flow of the former (Figs. 11(b), 11(d), and 11(f)) is lower than that of the latter (Figs. 11(a), 11(c), and 11(e)). Moreover, while the strongly inhibited traffic cases share some trend similarity with the weakly inhibited traffic cases, they also exhibit some peculiarities. These peculiarities are mostly associated with the difference in flow behavior around μ_c. This appears to be a result of the F1 case being more radically affected by size distribution under strongly inhibited traffic conditions. Therefore, we see that for the left-skewed traffic, the extent to which the F1 case exceeds the other cases at μ_c is less. Moving over to the balanced traffic case, the critical flow point for the F1 case is less compared to the flexible traffic cases, where we observe that critical flow values for the F2 and F3 cases are nearly the same. For right-skewed traffic, the F1 case exhibits a considerably lower flow at μ_c than those of the F2 and F3 cases.

All these factors reinforce the idea that the fixed arrival strategy (F1) tends to be sensitive to changes in arrival conditions. Conversely, we may describe the flexible arrival strategies (F2 and F3) as being inherently robust, in that they are less affected by variation in size distribution and traffic mobility. A possible reason behind this robustness is the pseudo-random nature of their operation. In other words, the availability of route options in flexible strategies mitigates the constraints of the spacing requirements associated with size distribution as well as aircraft mobility.

Fig. 12 shows the average speed characteristics of different flexibility indices under the size distributions considered. To aid our discussion, we define the first point of intersection between the lines of the average speed of the fixed strategy (F1) and the average speed of the flexible strategies (F2 and F3) to be μ_A and the second point of intersection to be μ_B. For left-skewed traffic (Fig. 12(a)), F1, F2, and F3 cases have similar average speed values at low μ ($\mu < \mu_A$). This corresponds to the free flow behavior of F1, F2, and F3 cases at low μ described above. Between μ_A and μ_1, the flexible strategies decelerate more steeply than the fixed strategy, before switching to a gentler deceleration mode. This transition in deceleration rates highlights the impact of flow reversal on average traffic speed for flexible strategies. In other words, the momentary increase in flow within the organized flow region (see Fig. 6(b)) causes a change in deceleration dynamics. This may be attributed to the traffic being affected by aircraft clustering around preferred waypoints. This tends to slow them down within this TMA occupancy window (which corresponds to the organized flow zone), before the traffic becomes saturated. For the fixed strategy, the average speed reduces continuously between μ_A and μ_B. This

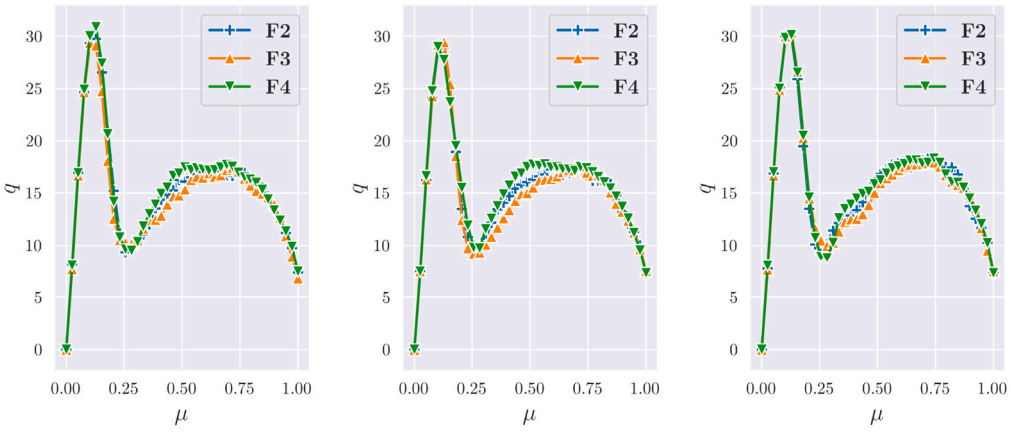

(a) Default configuration (b) Reshuffled configuration 1 (c) Reshuffled configuration 2

Fig. 13. Flow behavior for different waypoint configurations.

way, the transition from high deceleration rate to low deceleration rate is not sharply defined, compared to the fixed strategies. The foregoing dynamics are also observed when we examine the deceleration of balanced traffic across F1, F2, and F3 cases, except for two key differences (Fig. 12(b)). The first difference is the clear separation of the fixed and flexible strategies at low μ. As previously discussed, this may be attributed to the sensitivity of F1 case to the balanced traffic, leading to a notable downward shift in its speed in low μ. The second difference observed is the substantial shrinking of the gap between μ_A and μ_B. This is also traceable to the downward shift in the overall trend of F1 case. For the right-skewed traffic (Fig. 12(c)), we see that speed reduction due to the traffic mix substantially affects the average speed of the F1 case, such that the strategies only coincide at μ_1. In this case, the average speeds of the flexible strategies entirely exceed that of the fixed strategy at all points along the TMA occupancy axis.

One prominent feature across different size distributions is the almost identical behavior of the flexible strategies (recall that we have a similar observation on Fig. 7). It is important to investigate whether this similarity is caused by a certain model setup (e.g., waypoint configuration used in this study) or whether the higher level of flexibility does not manifest in different traffic flows. In order to verify these propositions, we conduct further analyses. First, we extend the flexibility index to fourth order (F4) for the current waypoint configuration. The outcome of this analysis should indicate whether the similarity between F2 and F3 is a random outcome or a feature of the model. Second, we reshuffle the waypoint arrangement in order to isolate flow dependence on a certain waypoint configuration. In particular, the waypoint configuration is reshuffled twice and we simulate the traffic for each case in order to ascertain the outcome. The results of these simulations are presented in Fig. 13. Fig. 13(a) shows the flow behaviors under F2, F3, and F4 cases using the default waypoint configuration that is used to obtain other results presented in this paper, whereas Figs. 13(b) and 13(c) show the flow behaviors for the two instances of reshuffled waypoints. We see from these figures that the flow behaviors are still similar, with only minimum differences. Considering this similarity, it appears that while the presence of flexibility affects traffic flow, its effect is independent of the degree of flexibility. Having eliminated strategy dependence and configuration dependence as causes, something more inherent in the model could be responsible for this behavior. It is most likely that this phenomenon is caused by the mobility constraint imposed by aircraft population in a local neighborhood. More clearly stated, an aircraft may have the impetus to navigate towards the TMA exit using several waypoints, but its inhibitive interaction with other aircraft in its immediate neighborhood may limit how far it can go, thus restricting it to use a closer waypoint. This constraint, which is due to localized traffic dynamics, could limit the changes that might otherwise accompany a variation of route options.

3.3. Transition dynamics

Fig. 14 depicts the relationship between flow peaks and their points of occurrence relative to TMA occupancy, where the y-axis indicates the flow q when the transition point μ_c and secondary peak μ_2 (if applicable, which excludes cases with fixed strategy) occur (obtained from Figs. 7 and 11). The purpose of the comparison is to show the sensitivity of the arrival strategy to traffic mix and arrival conditions.

We observe that the value of flow at μ_c of weakly inhibited traffic is generally higher than that of strongly inhibited traffic, thanks to the high mobility associated with weakly inhibited traffic as discussed in Sections 3.1 and 3.2. Also, we observe that the highest flow is obtained with the left-skewed traffic using the F1 strategy under weakly inhibited conditions. In this configuration, traffic mobility drives aircraft into more areas within the airspace, before flow transition occurs. This implies that left-skewed traffic under the fixed strategy in nominal conditions favors capacity utilization. Another observation is that a strongly inhibited case has comparable transition flow performance as some weakly inhibited cases (circled in black within the overlap band A in Fig. 14). On

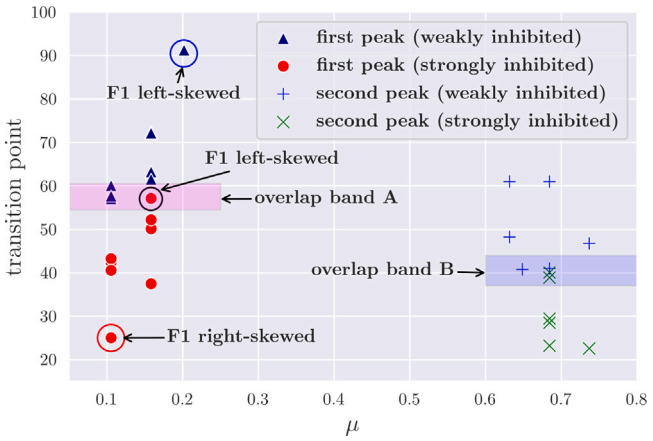

Fig. 14. The transition point of all cases, for weakly inhibited and strongly inhibited traffic scenarios.

closer examination, this point turns out to be associated with left-skewed traffic under the F1 strategy. Moreover, we see that the scenario with the least flow at the transition point is the strongly inhibited case of the right-skewed size distribution that employs the fixed strategy (F1). The wide range between transition points of the F1 case under different conditions (the points circled in red and blue respectively, in Fig. 14) further highlights the sensitivity of the fixed strategy to aircraft size distribution and arrival conditions.

The distribution of secondary peak points (μ_2) is presented on the right hand side of Fig. 14. In a manner similar to the distribution of critical points (μ_c) on the left hand side of the figure, weakly inhibited traffic generally has higher secondary peak flow values, compared to strongly inhibited traffic. We also have an area where weakly inhibited and strongly inhibited cases have similar flow values for the secondary peaks. This is indicated as *overlap band B*. The cases that fall in this region are the weakly inhibited, right-skewed traffic scenarios, as well as the left-skewed traffic scenarios that are strongly inhibited. These observations reveal the benefit that can be obtained from the appropriate arrival strategy, despite poor traffic mobility.

4. Conclusion

This paper investigated the impact of aircraft size distribution and navigation flexibility (in terms of waypoint selection) on TMA arrival traffic using a CA model. Our findings showed that a fixed strategy exhibited gentle transition behavior between free and congested flow zones. Although traffic under the fixed strategy saturated the TMA monotonously, it exhibited greater sensitivity to arrival traffic mix due to limited route options. On the other hand, traffic under the flexible arrival strategy saturated the TMA non-monotonically without showing substantial sensitivity to the arrival traffic mix. The post-peak non-monotonicity of the flexible strategy constituted the *organized flow zone*, where aircraft clustering around waypoints and the TMA exit led to a momentary rise in traffic flow, before entering the traffic saturation stage. Our study also revealed that having a higher degree of flexibility did not really affect traffic flow, due to the constraint imposed by localized traffic dynamics.

These insights suggest that a fixed arrival strategy will be more suitable to a traffic scenario that has mostly small and medium sized aircraft, owing to gentler transition around the critical flow state. However, the flexible strategy will better fit a traffic dominated by a mixture of large and small aircraft. This may be attributed to the fact that it better facilitates efficient flow when the spacing between aircraft is greater. Based on our observations, adopting a mixed strategy—by implementing the fixed and flexible arrival strategies before and after passing through the flow transition point, respectively—would be beneficial. Moreover, the occurrence of the organized flow zone, its precipitation around waypoints, and its role in setting the stage for TMA saturation suggest that the number and relative arrangement of waypoints play a critical role in traffic evolution within TMA.

The work presented herein has demonstrated the use of a statistical physics method to reveal macroscopic behaviors in the TMA by modeling its microscopic interactions. In particular, this work has shown how CA can be leveraged to model dynamic environments affected by multiple interacting parameters and constraints. Potential applications beyond air transportation modeling cut across physical systems that have well-defined terrain constraints or characterized by converging paths in a controlled environment, such as traffic behavior at road intersections and future urban air mobility systems. While CA model only serves as an abstraction of real-world systems, setting the model to fit the systems as closely as possible is imperative.

CRediT authorship contribution statement

Ikeoluwa Ireoluwa Ogedengbe: Writing – original draft, Visualization, Methodology, Investigation, Formal analysis, Conceptualization. **Tak Shing Tai:** Writing – review & editing, Methodology, Formal analysis. **K.Y. Michael Wong:** Supervision, Methodology, Funding acquisition, Conceptualization. **Rhea P. Liem:** Writing – review & editing, Supervision, Project administration, Methodology, Funding acquisition, Conceptualization.

Funding statement

The work was supported by the Innovation and Technology Commission (ITC) (Project No. ITS/016/20). Dr Tai is grateful for the postdoctoral fellowship supported by the Research Talent Hub under ITC (Project No. PiH/068/22).

Declaration of competing interest

The authors declare that they have no known competing financial interests or personal relationships that could have appeared to influence the work reported in this paper.

Data availability

No data was used for the research described in the article.

References

[1] G. Atef, F. Ken, An assessment of the impacts of congestion delay at major hubs to airlines and passengers, J. Aviat./ Aerosp. Educ. Res. 2 (1992) 17–23, http://dx.doi.org/10.15394/jaaer.1992.1071.
[2] P. Roosens, Congestion and air transport: A challenging phenomenon, Eur. J. Transp. Infrastruct. Res. 8 (2008) 137–146, http://dx.doi.org/10.18757/ejtir.2008.8.2.3338.
[3] B. Vaaben, J. Larsen, Mitigation of airspace congestion impact on airline networks, J. Air Transp. Manag. 47 (2015) 54–65, http://dx.doi.org/10.1016/j.jairtraman.2015.04.002.
[4] I. Ostroumov, N. Kuzmenko, Statistical analysis and flight route extraction from automatic dependent surveillance-broadcast data, in: 2022 Integrated Communication, Navigation and Surveillance Conference, ICNS, 2022, pp. i–ix, http://dx.doi.org/10.1109/ICNS54818.2022.9771515.
[5] M.C.R. Murça, C. Müller, Control-based optimization approach for aircraft scheduling in a terminal area with alternative arrival routes, Transp. Res. Part E: Logist. Transp. Rev. 73 (2015) 96–113, http://dx.doi.org/10.1016/j.tre.2014.11.004.
[6] L. Man, An agent-based approach to automated merge 4D arrival trajectories in busy terminal maneuvering area, Procedia Eng. 99 (2015) 233–243, http://dx.doi.org/10.1016/j.proeng.2014.12.531.
[7] C. Zuniga, D. Delahaye, M.A. Piera, Integrating and sequencing flows in terminal maneuvering area by evolutionary algorithms, in: 2011 IEEE/AIAA 30th Digital Avionics Systems Conference, IEEE, 2011, pp. 2A1–1, http://dx.doi.org/10.1109/DASC.2011.6095980.
[8] R. Coppenbarger, R. Lanier, D. Sweet, S. Dorsky, Design and development of the en route descent advisor (EDA) for conflict-free arrival metering, in: AIAA Guidance, Navigation, and Control Conference and Exhibit, 2004, p. 4875, http://dx.doi.org/10.2514/6.2004-4875.
[9] Á. Rodríguez-Sanz, D.Á. Álvarez, F.G. Comendador, R.A. Valdés, J. Pérez-Castán, M.N. Godoy, Air traffic management based on 4D trajectories: a reliability analysis using multi-state systems theory, Transp. Res. Procedia 33 (2018) 355–362, http://dx.doi.org/10.1016/j.trpro.2018.11.001.
[10] W. Zeng, X. Chu, Z. Xu, Y. Liu, Z. Quan, Aircraft 4D trajectory prediction in civil aviation: A review, Aerospace 9 (2) (2022) 91, http://dx.doi.org/10.3390/aerospace9020091.
[11] H. Khadilkar, H. Balakrishnan, Network congestion control of airport surface operations, J. Guid. Control Dyn. 37 (3) (2014) 933–940, http://dx.doi.org/10.2514/1.57850.
[12] M.K. El Mahrsi, C. Andrieu, E. Côme, Z. Bezza, L. Oukhellou, F. Rossi, Traffic characterization on airport surface using aircraft ground trajectories, in: 2018 21st International Conference on Intelligent Transportation Systems, ITSC, IEEE, 2018, pp. 3879–3885, http://dx.doi.org/10.1109/ITSC.2018.8569350.
[13] G.N. Lui, K.K. Hon, R.P. Liem, Weather impact quantification on airport arrival on-time performance through a Bayesian statistics modeling approach, Transp. Res. Part C: Emerg. Technol. 143 (2022) 103811, http://dx.doi.org/10.1016/j.trc.2022.103811.
[14] Y. Wang, Y. Zhang, Prediction of runway configurations and airport acceptance rates for multi-airport system using gridded weather forecast, Transp. Res. Part C: Emerg. Technol. 125 (2021) 103049, http://dx.doi.org/10.1016/j.trc.2021.103049.
[15] T. Krauth, A. Lafage, J. Morio, X. Olive, M. Waltert, Deep generative modelling of aircraft trajectories in terminal maneuvering areas, Mach. Learn. Appl. 11 (2023) 100446, http://dx.doi.org/10.1016/j.mlwa.2022.100446.
[16] W. Zeng, Z. Xu, Z. Cai, X. Chu, X. Lu, Aircraft trajectory clustering in terminal airspace based on deep autoencoder and Gaussian mixture model, Aerospace 8 (9) (2021) 266, http://dx.doi.org/10.3390/aerospace8090266.
[17] X. Chu, X. Tan, W. Zeng, A clustering ensemble method of aircraft trajectory based on the similarity matrix, Aerospace 9 (5) (2022) 269, http://dx.doi.org/10.3390/aerospace9050269.
[18] M.C.R. Murca, R.J. Hansman, L. Li, P. Ren, Flight trajectory data analytics for characterization of air traffic flows: A comparative analysis of terminal area operations between new york, Hong Kong and sao paulo, Transp. Res. Part C: Emerg. Technol. 97 (2018) 324–347, http://dx.doi.org/10.1016/j.trc.2018.10.021.
[19] S. Sidiropoulos, A. Majumdar, K. Han, A framework for the optimization of terminal airspace operations in multi-airport systems, Transp. Res. Part B: Methodol. 110 (2018) 160–187, http://dx.doi.org/10.1016/j.trb.2018.02.010.
[20] M. Yousefzadeh Aghdam, S.R. Kamel Tabbakh, S.J. Mahdavi Chabok, M. Kheyrabadi, Optimization of air traffic management efficiency based on deep learning enriched by the long short-term memory (LSTM) and extreme learning machine (ELM), J. Big Data 8 (1) (2021) 1–26, http://dx.doi.org/10.1186/s40537-021-00438-6.
[21] Y. Xie, N. Pongsakornsathien, A. Gardi, R. Sabatini, Explanation of machine-learning solutions in air-traffic management, Aerospace 8 (8) (2021) 224, http://dx.doi.org/10.3390/aerospace8080224.
[22] L. Lacasa, M. Cea, M. Zanin, Jamming transition in air transportation networks, Phys. A 388 (18) (2009) 3948–3954, http://dx.doi.org/10.1016/j.physa.2009.06.005.
[23] J. Ma, D. Delahaye, M. Sbihi, P. Scala, M.A. Mujica Mota, Integrated optimization of terminal maneuvering area and airport at the macroscopic level, Transp. Res. Part C: Emerg. Technol. 98 (2019) 338–357, http://dx.doi.org/10.1016/j.trc.2018.12.006.
[24] H. Liu, X. Zhang, X. Zhang, Exploring dynamic evolution and fluctuation characteristics of air traffic flow volume time series: A single waypoint case, Phys. A 503 (2018) 560–571, http://dx.doi.org/10.1016/j.physa.2018.02.030.
[25] E. Itoh, M. Mitici, Queue-based modeling of the aircraft arrival process at a single airport, Aerospace 6 (10) (2019) 103, http://dx.doi.org/10.3390/aerospace6100103.
[26] K. Higasa, E. Itoh, Controlling aircraft inter-arrival time to reduce arrival traffic delay via a queue-based integer programming approach, Aerospace 9 (11) (2022) 663, http://dx.doi.org/10.3390/aerospace9110663.

[27] T.M. Sobh, R. Bajcsy, A model for visual observation under uncertainty, in: IEEE Symposium on Computer-Aided Control System Design, IEEE, 1992, pp. 269–274, http://dx.doi.org/10.1109/CACSD.1992.274421.
[28] W. Knospe, L. Santen, A. Schadschneider, M. Schreckenberg, Towards a realistic microscopic description of highway traffic, J. Phys. A: Math. Gen. 33 (48) (2000) L477, http://dx.doi.org/10.1088/0305-4470/33/48/103.
[29] E.C. Gabrick, P.R. Protachevicz, A.M. Batista, K.C. Iarosz, S.L. de Souza, A.C. Almeida, J.D. Szezech, M. Mugnaine, I.L. Caldas, Effect of two vaccine doses in the SEIR epidemic model using a stochastic cellular automaton, Phys. A 597 (2022) 127–258, http://dx.doi.org/10.1016/j.physa.2022.127258.
[30] X. Li, F. Guo, H. Kuang, Z. Geng, Y. Fan, An extended cost potential field cellular automaton model for pedestrian evacuation considering the restriction of visual field, Phys. A 515 (2019) 47–56, http://dx.doi.org/10.1016/j.physa.2018.09.145.
[31] M. Hemmo, O. Shenker, The emergence of macroscopic regularity, Mind Soc. 14 (2015) 221–244.
[32] S.Y. Auyang, Foundations of Complex-System Theories: in Economics, Evolutionary Biology, and Statistical Physics, Cambridge University Press, 1998.
[33] J. Kwapień, S. Drożdż, Physical approach to complex systems, Phys. Rep. 515 (3–4) (2012) 115–226.
[34] C.J. Puccia, R. Levins, Qualitative Modeling of Complex Systems: An Introduction to Loop Analysis and Time Averaging, Harvard University Press, Cambridge, MA and London, England, 1985, http://dx.doi.org/10.4159/harvard.9780674435070.
[35] B. Chopard, A. Masselot, Cellular automata and lattice Boltzmann methods: a new approach to computational fluid dynamics and particle transport, Future Gener. Comput. Syst. 16 (2–3) (1999) 249–257, http://dx.doi.org/10.1016/S0167-739X(99)00050-3.
[36] H.J. Bussemaker, A. Deutsch, E. Geigant, Mean-field analysis of a dynamical phase transition in a cellular automaton model for collective motion, Phys. Rev. Lett. 78 (26) (1997) 5018, http://dx.doi.org/10.1103/PhysRevLett.78.5018.
[37] R. Jiang, Q. Wu, First order phase transition from free flow to synchronized flow in a cellular automata model, Eur. Phys. J. B- Condens. Matter Complex Syst. 46 (2005) 581–584, http://dx.doi.org/10.1140/epjb/e2005-00290-4.
[38] F. Polese, A. Payne, P. Frow, D. Sarno, S. Nenonen, Emergence and phase transitions in service ecosystems, J. Bus. Res. 127 (2021) 25–34, http://dx.doi.org/10.1016/j.jbusres.2020.11.067.
[39] Kai Nagel, Michael Schreckenberg, A cellular automaton model for freeway traffic, J. Physque I Fr. 2 (12) (1992) 2221–2229, http://dx.doi.org/10.1051/jp1:1992277.
[40] S. Wang, X. Cao, H. Li, Q. Li, X. Hang, Y. Wang, Air route network optimization in fragmented airspace based on cellular automata, Chin. J. Aeronaut. 30 (3) (2017) 1184–1195, http://dx.doi.org/10.1016/j.cja.2017.04.002.
[41] S.-j. Wang, Y.-h. Gong, Research on air route network nodes optimization with avoiding the three areas, Saf. Sci. 66 (2014) 9–18, http://dx.doi.org/10.1016/j.ssci.2014.01.008.
[42] S. Yu, X. Cao, M. Hu, W. Du, J. Zhang, A real-time schedule method for aircraft landing scheduling problem based on cellular automaton, in: Proceedings of the First ACM/SIGEVO Summit on Genetic and Evolutionary Computation, Association for Computing Machinery, 2009, pp. 717–724, http://dx.doi.org/10.1145/1543834.1543932.
[43] T.S. Tai, C.H. Yeung, Global benefit of randomness in individual routing on transportation networks, Phys. Rev. E 100 (2019) 012311, http://dx.doi.org/10.1103/PhysRevE.100.012311.
[44] B.J. LuValle, The effects of boundary conditions on cellular automata, Complex Systems 28 (1) (2019) http://dx.doi.org/10.25088/ComplexSystems.28.1.97.
[45] T. Vranken, B. Sliwa, C. Wietfeld, M. Schreckenberg, Adapting a cellular automata model to describe heterogeneous traffic with human-driven, automated, and communicating automated vehicles, Phys. A 570 (2021) http://dx.doi.org/10.1016/j.physa.2021.125792.
[46] M. Rickert, K. Nagel, M. Schreckenberg, A. Latour, Two lane traffic simulations using cellular automata, Phys. A 231 (4) (1996) 534–550, http://dx.doi.org/10.1016/0378-4371(95)00442-4.
[47] F. Enayatollahi, M.A. Atashgah, Wind effect analysis on air traffic congestion in terminal area via cellular automata, Aviation 22 (3) (2018) 102–114, http://dx.doi.org/10.3846/aviation.2018.6252.
[48] C.H. Nguyen, R.P. Liem, Multi-aircraft attention-based model for perceptive arrival transit time prediction, Adv. Eng. Inform. 64 (2025) 103067, http://dx.doi.org/10.1016/j.aei.2024.103067.
[49] I. Dhief, M. Feroskhan, S. Alam, N. Lilith, D. Delahaye, Meta-heuristics approach for arrival sequencing and delay absorption through automated vectoring, in: 2023 IEEE Congress on Evolutionary Computation, CEC, Institute of Electrical and Electronic Engineers, 2023, pp. 1–8, http://dx.doi.org/10.1109/CEC53210.2023.10254077.
[50] Radar vectoring procedure and method — wiki.ivao.aero, 2016, https://wiki.ivao.aero/en/home/training/documentation/Radar_vectoring_procedure_and_method. (Accessed 19 December 2024).
[51] D. Wilken, P. Berster, M.C. Gelhausen, New empirical evidence on airport capacity utilisation: Relationships between hourly and annual air traffic volumes, Res. Transp. Bus. Manag. 1 (1) (2011) 118–127, http://dx.doi.org/10.1016/j.rtbm.2011.06.008.
[52] L. Audenaerd, D. Domino, S. Lang, C. Lunsford, A.P. Smith, J. Tittsworth, Increasing airport arrival capacity in NextGen with wake turbulence avoidance, in: 2009 Integrated Communications, Navigation and Surveillance Conference, IEEE, 2009, pp. 1–15, http://dx.doi.org/10.1109/ICNSURV.2009.5172828.
[53] F. Siebel, W. Mauser, On the fundamental diagram of traffic flow, SIAM J. Appl. Math. 66 (4) (2006) 1150–1162, http://dx.doi.org/10.1137/050627113.
[54] B.S. Kerner, Experimental features of self-organization in traffic flow, Phys. Rev. Lett. 81 (17) (1998) 3797, http://dx.doi.org/10.1103/PhysRevLett.81.3797.
[55] B.S. Kerner, Criticism of generally accepted fundamentals and methodologies of traffic and transportation theory: A brief review, Phys. A 392 (21) (2013) 5261–5282, http://dx.doi.org/10.1016/j.physa.2013.06.004.